Ferroresonance

by Donald M. Scoggin
James E. Hall, Jr.

This paper describes a mathematical model for ferroresonant circuits that addresses some of the deficiencies of earlier analyses of ferroresonant regulators. Derived using piecewise-linear, normalized differential equations, the model accommodates nonlinear behavior and predicts circuit performance in terms of parameters such as line voltage, frequency, and load. A phase-plane analysis is used to simplify the determination of linear regions of operation between nonlinear events. Numerical solutions of the resulting equations are used to generate time-domain and parametric performance curves. The results compare well with experiments and suggest potential applications in the design of high-frequency voltage regulators.

Introduction

Ferroresonance and, in particular, the ferroresonant transformer have played an important role in the electronic and industrial communities for more than 40 years. The ferroresonant regulator has provided inexpensive and reliable line-voltage regulation for consumer, industrial, and data processing products. The technical papers describing its operation, however, are few and often conflicting. This paper briefly reviews general voltage regulators and the literature on ferroresonance, then develops a model to explain and simulate ferroresonant behavior more completely than these earlier descriptions.

In most electronic products, there exists a need to compensate for varying input voltage. Usually this is accomplished by linear, switching, or ferroresonant power supplies. The linear power supply uses a transistor in its active region to absorb variations in input. This regulator offers optimum performance at the expense of efficiency and relatively large size. A switching regulator gains its advantage by using a transistor as a high-frequency, theoretically nondissipative switch; it offers high performance but generates high levels of electromagnetic interference (EMI) and has relatively low reliability. (For a concise description of EMI and an alternate approach to dealing with it, see [1].) The ferroresonant regulator offers extreme reliability but, at the traditional operating frequency of 60 Hz, has the disadvantage of size and weight. We show here, however, that the phenomenon of ferroresonance can be used at higher frequencies to achieve the size and weight advantages while retaining the useful features of the 60-Hz devices. (There are also other, quasi-resonant designs that are receiving research attention [2, 3].)

Ferroresonance involves the use of square-loop magnetic material to limit the operating flux in a magnetic element. This results in a degree of voltage regulation; however, saturation of the magnetic device leads to nonlinear circuit behavior that linear methods of analysis can only approximate. A review of existing papers [4–6] nevertheless indicates that the use of linear techniques to achieve approximate models is prevalent.

Basu [4], Friedman [5], Kakalec and Hart [6], Keefe [7], and others use phasor analysis. Often, as in Kakalec, the equations are modified by empirical data. These models are

©**Copyright** 1987 by International Business Machines Corporation. Copying in printed form for private use is permitted without payment of royalty provided that (1) each reproduction is done without alteration and (2) the *Journal* reference and IBM copyright notice are included on the first page. The title and abstract, but no other portions, of this paper may be copied or distributed royalty free without further permission by computer-based and other information-service systems. Permission to *republish* any other portion of this paper must be obtained from the Editor.

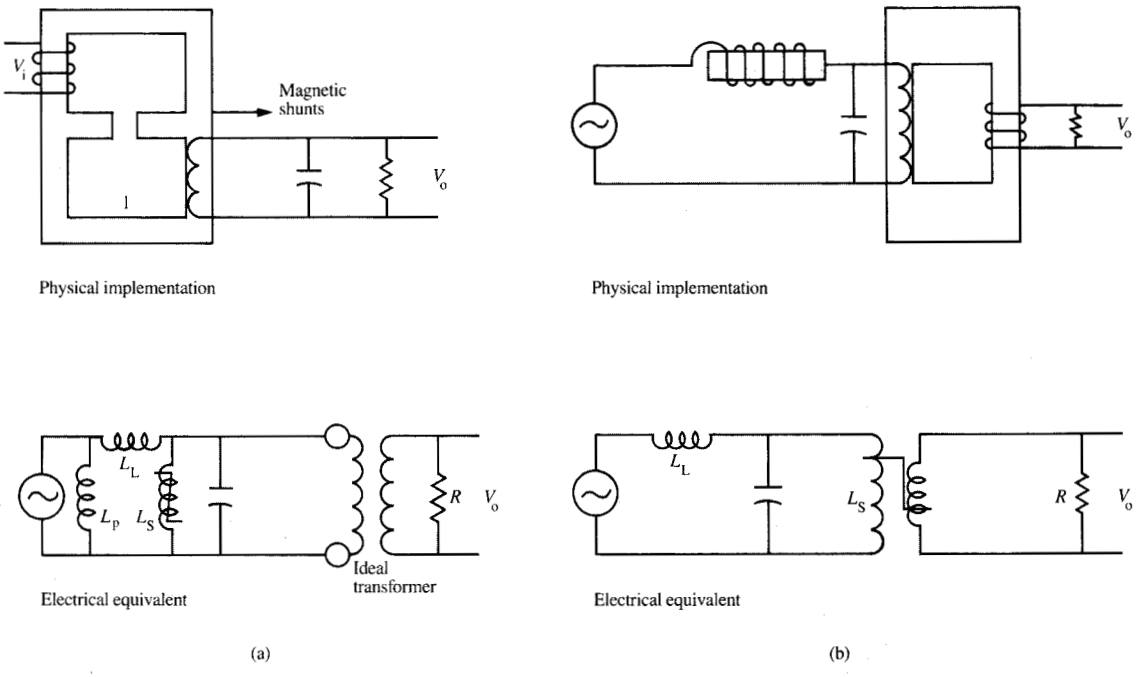

Figure 1

Two popular ferroresonant circuit configurations.

the accepted industrial standards and do in fact yield acceptable design starting points, but usually they are only the first step in an iterative process. More desirable would be a model that accepts nonlinear behavior and predicts circuit performance in terms of parameters such as line voltage, frequency, or load (where load is varied). Such a model is proposed in this paper.

Behavior of ferroresonant circuits

The ferroresonant circuit can be implemented in many ways. Two popular versions are shown in **Figure 1** with their physical and electrical representations.

Each circuit consists of a linear inductor L_L, a saturating inductor L_S, a capacitor in parallel with L_S, and a load resistor R.

Historically, the 60-Hz ferroresonant transformer has employed the configuration of Figure 1(a) because of the lower material and labor costs that can be achieved by incorporating the linear inductor and transformer into one assembly. However, as frequency is increased, the circuit of Figure 1(b) becomes more attractive due to the types and sizes of cores that can be used.

The duality of the circuits of Figure 1 is described by Biega [8] and Kakalec and Hart [6]. Briefly, in Figure 1(a), the linear inductor is realized by placing a magnetic shunt between the primary and secondary windings. This shunt creates a path for flux and is modeled as a series inductance. This is analogous to the standard approach of modeling the leakage flux of a linear transformer as a series inductance. The leakage inductance of the linear transformer is usually reflected arbitrarily to one side or split equally. This is justified since its effect can be shifted or split without altering circuit performance. However, the shunts in Figure 1(a) create a flux path (leakage inductance) between windings. Thus, the resulting leakage inductance is more accurately modeled by inserting it between windings. In most analyses [4–6], the circuit of Figure 1(a) is reduced to that of Figure 1(b) by referring elements to one side and neglecting magnetizing inductance [L_p in Figure 1(a)].

The basic operation of a ferroresonant regulator can be described as follows. If the saturable inductor of Figure 1(b) has a magnetizing curve (or hysteresis loop; the curve for square-loop material is shown in **Figure 2**), then the voltage across the device can be written as

$$e(t) = N\frac{d\psi}{dt}, \tag{1}$$

where N = number of turns, ψ = magnetic flux, and t = time. Integrating and assuming that the core saturates prior to the end of a half-cycle yields

$$V_o = \frac{2}{T}\int_0^{T/2} e(t)dt = \frac{2N}{T}\int_{-\psi_{max}}^{\psi_{max}} d\psi; \tag{2}$$

$$V_o = 4Nf\psi_{max}, \tag{3}$$

where V_o is the half-cycle average output voltage, $T/2$ is the time required for one half-cycle of operation, ψ_{max} is the maximum flux during the half-cycle, and $f(=1/T)$ is the frequency.

Equation (3) states that the half-cycle average value of the output voltage V_o is constant if the input is driven from a constant-frequency source and the flux changes by $2\psi_{max}$ each half-cycle. However, $e(t)$, the instantaneous value for V_o, can vary.

An observation can be made that a given core can be driven between saturation limits without the linear inductor or capacitor. However, the need for efficient power transfer necessitates an element that will limit peak line current when L_S saturates. As will be seen, the use of such a linear element extends the useful operating range of the circuit. The role of the inductor is unique in this topology. The volt-second limiting and voltage switching action of L_S forces L_L to act as a volt-second buffer for the circuit. If the average value of the input voltage exceeds the average value of the output voltage, then L_L will act to absorb the excess volt-seconds. If the average input voltage is too low, then the inductor is "pumped" and made to act as a source of stored energy, to maintain the required volt-second content of the output voltage.

By assuming steady-state operation, the circuit can be described as follows. Prior to saturation, the current in the saturable reactor (inductor) L_S is essentially zero, since it has a very high inductance. At time t_1, the core saturates (**Figure 3**), and the inductance L_S is reduced to a small value. A current pulse I_{LS} begins to flow through the saturated inductor. It would, in a linear circuit, ring at a frequency of

$$f \approx \frac{1}{2\pi\sqrt{L_{S(Sat)}C}}. \tag{4}$$

However, as the current approaches 0, L_S comes out of saturation, stopping the oscillation (t_2 in Figure 3). The voltage across the capacitor is reversed, and remains at this polarity until the end of the half-cycle, when the saturation occurs again (t_3 in Figure 3).

The saturation of the reactor and the resulting current pulse have a squaring effect on the output. This squaring causes phasor analysis to be an approximate technique at best, since phasors are applicable only to linear, steady-state, sinusoidal systems. The standard methods of describing circuit operation using phasor techniques are not adequate to predict operation over a a complete range of circuit operation. In real devices, the current and voltage waveforms range from sinusoidal to rectangular depending on input voltage, frequency, and load.

The square-wave output is ideal for filtering purposes. Additionally, the input impedance of these devices results in a low-pass LC filter behavior, making it a good buffer for high-frequency noise. Also, the circuit is not sensitive to waveform distortions because it integrates the input waveform. The volt-seconds of the input waveform must, however, be sufficient to saturate the inductor L_S.

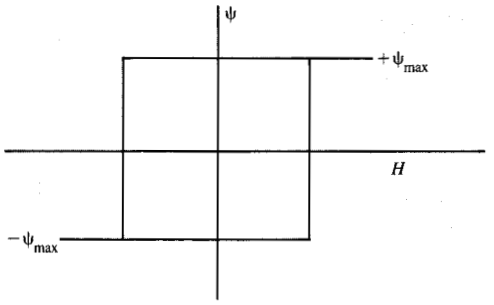

Figure 2

Magnetizing curve for square-loop material.

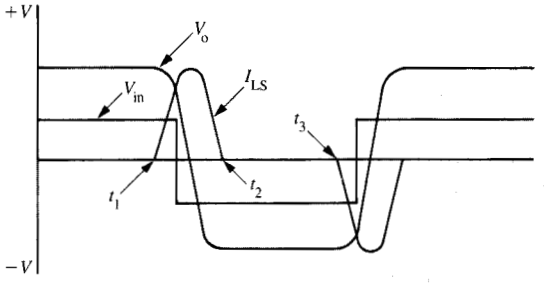

Figure 3

Waveforms for a ferroresonant circuit.

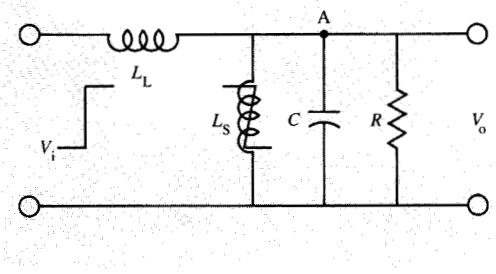

Figure 4

Ferroresonant circuit model.

The term "ferroresonance," used to describe circuit operation, is misleading. The circuit does not operate like a linear resonant circuit, but is instead a volt-second limiter. The circuit is tuned about a certain frequency to achieve optimum behavior but does not oscillate in a linear mode. We note that this circuit, given specific component values, can be solved by computerized analysis programs, e.g. [9, 10], and additional second-order effects, such as stray capacitance, could be included. (For a discussion of this approach, see [11].) However, we seek a more general result.

A model is needed that predicts circuit operation under various operating conditions. The model should be normalized to allow circuit parameters to be varied without difficulty, and it should closely track observed behavior. The derivation and justification of such a model are now shown.

System analysis

• *Mathematical circuit analysis*

The model in **Figure 4** represents the desired ferroresonant circuit, which can be described mathematically with a second-order linear differential equation. This approach is justified if the resulting equation is reset at each nonlinear occurrence, and the nonlinear result is reduced to a series of linear segments. This is accomplished by resetting the initial conditions of the equations.

A Kirchoff nodal equation in one of the linear segments describing the circuit can be written about node A as follows:

$$\frac{1}{L_L}\int [V_i(t) - V_o(t)]dt + I_{L0} = C\frac{dV_o(t)}{dt} + \frac{1}{L_S}\int V_o(t)dt + \frac{V_o(t)}{R_L} + I_{LS0}, \quad (5)$$

where I_{L0} is the initial current in linear inductor L_L and I_{LS0} is the initial current in saturable inductor L_S. [$V_i(t)$ and $V_o(t)$ are the time-varying input and output, respectively, and are not to be confused with the terms defined earlier for average values.] Grouping terms, we obtain the following:

$$\frac{1}{L_L C}\int V_i(t)dt + \frac{I_{L0}}{C} = \frac{dV_o(t)}{dt} + \frac{V_o(t)}{RC} + \left(\frac{1}{L_S} + \frac{1}{L_L}\right)\left(\frac{1}{C}\right)\int V_o(t)dt + \frac{1}{C}I_{LS0}. \quad (6)$$

The terms I_{L0} and I_{LS0} allow the equations to be reset at each nonlinear transition. This is critical in the analysis since this allows us to treat the nonlinear system with ordinary differential equations. Furthermore, the term I_{LS0} is neglected, since it can be assumed to be negligible when L_S is not saturated. This assumption is discussed in the phase-plane analysis and symmetry arguments given later in this paper.

From the previous discussion, it is known that the variable of interest is the flux in the saturable inductor L_S. As a result, a substitution can be made in Equation (6) to obtain the output voltage in terms of flux. This is possible since Faraday's law states that

$$V_o(t) = N\frac{d\psi_S}{dt}, \quad (7)$$

where ψ_S is the magnetic flux in saturable inductor L_S.

Substituting Equation (7) into Equation (6) gives

$$\frac{1}{L_L C}\int V_i(t)dt + \frac{I_{L0}}{C} = \frac{d}{dt}\left(\frac{Nd\psi_S}{dt}\right) + \left(\frac{N}{RC}\right)\frac{d\psi_S}{dt} + \frac{N}{C}\left(\frac{1}{L_S} + \frac{1}{L_L}\right)\int \frac{d\psi_S}{dt}dt, \quad (8)$$

$$\frac{1}{L_L C}\int V_i(t)dt + \frac{I_{L0}}{C} = \frac{Nd^2\psi_S}{dt^2} + \frac{N}{RC}\frac{d\psi_S}{dt} + \frac{N}{C}\left(\frac{1}{L_S} + \frac{1}{L_L}\right)\int_{\psi=\psi_0}^{\psi=\psi_S} d\psi_S, \quad (9)$$

and

$$\frac{1}{L_L C}\int V_i(t)dt + \frac{I_{L0}}{C} = \frac{Nd^2\psi}{dt^2} + \frac{N}{RC}\frac{d\psi_S}{dt} + \left(\frac{1}{L_S} + \frac{1}{L_L}\right)(\psi_S - \psi_0)\frac{N}{C}. \quad (10)$$

At this point, we define parameters for ease of analysis:

$$\omega_0^2 = \frac{1}{L_L C},$$

where ω_0 is the resonant frequency of the linear inductor and capacitor; and

$$\omega_S^2 = \frac{1}{L_S C},$$

where ω_S is the resonant frequency of the saturable inductor and capacitor. Then the quality factor Q can be written as

$$Q_0 = \frac{\omega_0 L_L}{R} = \frac{1}{\omega_0 C R}.$$

The quality factor Q relates load R to the values of L and C. As can be seen from the analysis, the values of L and C must meet two criteria. First, they must be selected from the standpoint of realizable frequencies (ω_S and ω_0). Second, they must be selected to meet the load requirements through the Q_0 relationship.

Substituting ω_0^2, ω_S^2, and Q_0 into Equation (10), we obtain

$$\omega_0^2 \int V_i(t)dt + \frac{I_{L0}}{C} = N\frac{d^2\psi_S}{dt^2} + NQ_0\omega_0\frac{d\psi_S}{dt} + N(\omega_0^2 + \omega_S^2)(\psi_S - \psi_0). \quad (11)$$

Equation (11) represents the circuit for any linear period of operation, and can be reset at each nonlinear event in the cycle by resetting the initial conditions. (It should be noted that a similar representation appears in the work edited by Katz [12]; there, however, the Q_0 term is not included and loading is therefore not taken into account.)

• *Circuit normalization*

At this point, it is desired to make the results general in nature and independent of particular circuit values. A normalized equation is needed. Normalization allows circuit parameters to be varied more easily. Begin by normalizing time and flux:

$$\text{normalized time} = \tau = \frac{\text{actual time}}{\text{resonant period of } \omega_0} = \frac{t}{(2\pi/\omega_0)} = \frac{\omega_0}{2\pi}t, \quad (12)$$

and

$$\text{normalized flux} = \chi = \frac{\text{actual flux in } L_S}{\text{saturation flux of } L_S} = \frac{\psi_S}{\psi_{max}}; \quad (13)$$

so

$$\frac{d\psi}{dt} = \left(\frac{\omega_0}{2\pi}\right)\frac{d\psi}{d\tau} \quad \text{and} \quad \frac{d^2\psi}{dt^2} = \left(\frac{\omega_0^2}{4\pi^2}\right)\frac{d^2\psi}{d\tau^2}. \quad (14)$$

Substituting Equations (12), (13), and (14) into Equation (11) gives

$$\frac{\omega_0^2 2\pi}{\omega_0}\int V_i(\tau)d\tau + \frac{I_{L0}}{C} = \left(\frac{N\psi_{max}\omega_0^2}{(2\pi)^2}\right)\frac{d^2\chi}{d\tau^2} + \left(\frac{N\omega_0^2 Q_0\psi_{max}}{2\pi}\right)\frac{d\chi}{d\tau} + N\psi_{max}(\omega_0^2 + \omega_S^2)(\chi - \chi_0). \quad (15)$$

Next divide by the coefficient of $d^2\chi/d\tau^2$, which results in

$$\frac{8\pi^3}{N\omega_0\psi_{max}}\int V_i(\tau)d\tau + \frac{4\pi^2 I_{L0}}{N\psi_{max}\omega_0^2 C} + \frac{(\omega_0^2 + \omega_S^2)(4\pi^2)\chi_0}{\omega_0^2} = \frac{d^2\chi}{d\tau^2} + 2\pi Q_0\frac{d\chi}{d\tau} + \frac{4\pi^2(\omega_0^2 + \omega_S^2)\chi}{\omega_0^2}. \quad (16)$$

Consider a bipolar square wave for the input waveform. Then define

$$V_{in} \text{ or, for convenience, } \alpha = \pm\frac{8\pi^3 V_i(\tau)}{N\omega_0\psi_{max}}, \quad (17)$$

where α is the normalized input and V_i is the amplitude of the input waveform. Making similar definitions,

$$\beta = \frac{4\pi^2(\omega_0^2 + \omega_S^2)}{\omega_0^2}, \quad (18)$$

$$I_{Ln0} = \frac{4\pi^2 I_{L0}}{N\psi_{max}\omega_0^2 C}, \quad (19)$$

and

$$Q_{n0} = \pi Q_0, \quad (20)$$

where β is the normalized natural circuit frequency, I_{Ln0} is the normalized inductor current at $\tau = 0$, and Q_{n0} is the normalized load (quality) factor.

The resulting differential equation can be written as

$$\alpha\tau + I_{Ln0} + \beta\chi_0 = \frac{d^2\chi}{d\tau^2} + 2Q_{n0}\frac{d\chi}{d\tau} + \beta\chi. \quad (21)$$

As desired, the resulting coefficients of the differential equation are dimensionless.

• *Solution of the system equation*

The general solution of Equation (21) is obtained by standard methods (see Appendix A) and is shown below:

$$\chi(\tau) = e^{-Q_{n0}\tau}\left\{\left(\frac{2Q_{n0}\alpha}{\beta^2} - \frac{I_{Ln0}}{\beta}\right)\cos\sigma\tau + \frac{1}{\sigma}\left[V_{on0} - \frac{I_{Ln0}Q_{n0}}{\beta} + \frac{\alpha}{\beta}\left(\frac{2Q_{n0}^2}{\beta} - 1\right)\right]\sin\sigma\tau\right\} + \frac{\alpha}{\beta}\tau + \frac{I_{Ln0}}{\beta} + \chi_0 - \frac{2Q_{n0}\alpha}{\beta^2}, \quad (22)$$

where V_{on0} is the normalized output voltage at $\tau = 0$, I_{Ln0} is the normalized linear inductor current at $\tau = 0$, χ_0 is the

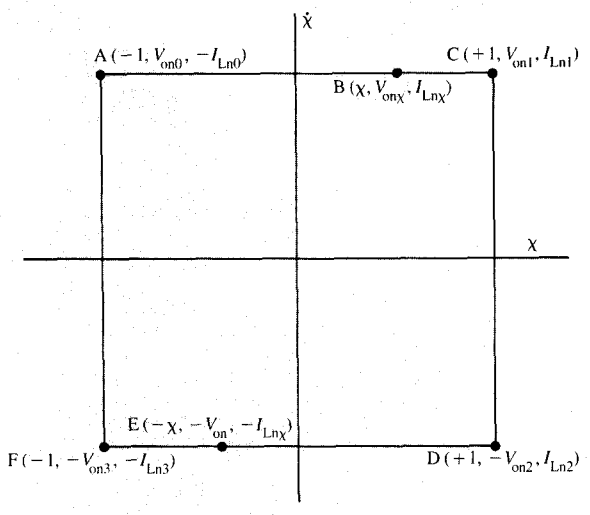

Figure 5

Phase plane for analysis of ferroresonant circuits. All units (flux, voltage, current) are normalized.

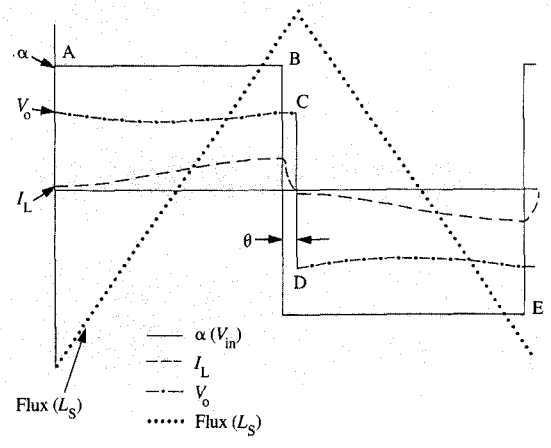

Figure 6

Time-domain plot of waveforms for nominal operating conditions: $\alpha = 0.7\,\alpha_{max}$; $Q = 0.2$; $\theta = 10°$; frequency = nominal.

normalized flux at $\tau = 0$, and

$$\sigma = \sqrt{\beta - Q_{n0}^2}.$$

Similarly, the output voltage, according to Faraday's law, can be written as the time derivative of the flux:

$$\dot{\chi}(\tau) = V_{on}(\tau)$$

$$= e^{-Q_{n0}\tau}\left[\left(V_{on0} - \frac{\alpha}{\beta}\right)\cos\sigma\tau - \frac{1}{\sigma}\left(Q_{n0}V_{on0} + \frac{Q_{n0}\alpha}{\beta} - I_{Ln0}\right)\sin\sigma\tau\right] + \frac{\alpha}{\beta}. \quad (23)$$

Both Equations (22) and (23) have terms for the linear inductor current. An expression for this circuit variable is needed in combination with Equations (22) and (23) to describe the circuit completely. By referring to the initial circuit schematic, the following equation can be written to describe the inductor current:

$$I_L = \frac{I}{L_L}\int [V_i(t) - V_o(t)]dt + I_{L0}$$

$$= \frac{I}{L_L}\int V_i(t)dt - \frac{I}{L_L}\int V_o(t)dt + I_{L0}. \quad (24)$$

It can be shown (see Appendix B) that this can be rewritten as

$$I_{Ln} = \alpha\tau - 4\pi^2(\chi - \chi_0) + I_{Ln0}, \quad (25)$$

where I_{Ln} is the normalized linear inductor current and I_{Ln0} is the normalized linear inductor current at $\tau = 0$. Equations (22), (23), and (25) are sufficient to describe the network. However, certain initial conditions must be determined in order to obtain particular solutions for a given system. Inspection of the flux and voltage equations reveals terms for initial linear inductor current I_{Ln0}, initial output voltage V_{on0}, and initial flux χ_0 in the saturable inductor L_S. These values are derived from analytical arguments and the property of phase-plane symmetry.

- *Phase-plane analysis*

The phase plane is a method of graphically observing the solutions of a second-order system. It is particularly helpful when dealing with nonlinear systems. The phase plane is represented as a plot of the derivative of a variable versus the variable. Saturating inductor flux and its time derivative, output voltage, are the two variables for the particular phase plane of our system, shown in **Figure 5**.

The horizontal axis represents flux and the vertical axis represents the time derivative of the flux (i.e., normalized voltage). For clarity, points in the phase plane are alphabetically labeled for later comparison to time-domain plots (**Figures 6**, **7**, and **8**). During ferroresonant operation, refer to negative flux saturation point A $(-1, V_{on0}, I_{Ln0})$ (or $t = 0$ for time domain; see Figure 6) and proceed left to right toward positive saturation, represented by point C $(+1, V_{on1}, I_{Ln1})$. Point B $(\chi, V_{on\chi}, I_{Ln\chi})$ represents the point at which the input voltage waveform switches polarity. At

this point, we make the general observation that the input voltage switches prior to the saturation of the inductor. This is an observed phenomenon and is useful in completing the analysis. The amount of delay is referred to as the phase lag. The phase lag is represented by the time it takes the saturable reactor flux to move from point B (χ, $V_{on\chi}$, $I_{Ln\chi}$) to positive saturation, point C (+1, V_{on1}, I_{Ln1}). Following the input polarity change, the "resonant" capacitor drives the output to the saturation point. The capacitor discharges, driving the system to point D (+1, $-V_{on2}$, I_{Ln1}), and the cycle moves along the bottom segment to point E ($-\chi$, $-V_{on\chi}$, $-I_{Ln\chi}$), where the input switches again.

For a stable oscillatory system, we can surmise several characteristics that can simplify the analysis; these are presented in Appendix C. They allow the treatment of only the first two segments. The first segment is the trajectory from negative saturation to point B, where the input switches. The next segment is from point B to point C. By forcing convergence of these two segments, the performance of the entire system can be determined.

At this point, calculations and conclusions can be summarized. Expressions for output voltage, flux, and linear inductor current have been obtained. Also, the initial and final values of flux (+1 or −1) are known from symmetry. However, initial values are not known for output voltage or linear inductor current. Additionally, Equations (22), (23), and (25) are only valid for the first segment, prior to the polarity change of the input waveform. The equations are reset at this point and applied over segment B–C. The phase lag from B to C is defined as θ degrees, or τ_θ in normalized time units. The phase angle and the initial values of output voltage and input current in this second segment must be determined. It can be shown (Appendix D) that the initial inductor (input) current can be defined in terms of the phase angle as

$$I_{Ln0} = 4\pi^2 - \alpha(\text{Period}/4 - \tau_\theta), \tag{26}$$

where Period is the cycle of oscillation (e.g., nominal Period = 1).

Thus, the problem is reduced to finding values for θ and the initial output voltage. Previous arguments (see Appendix C) have determined that $V_{on0} = V_{on1}$.

Expressions can be written for voltage and flux for the first and second segments. These equations, coupled with the linear inductor current equations, are sufficient to define the system completely.

The family of equations can be solved to yield two expressions for the initial output voltage in terms of τ_θ, the single unknown (see Appendix E):

$$V^1_{on0} = f_1(\tau_\theta)$$

and

$$V^2_{on0} = f_2(\tau_\theta).$$

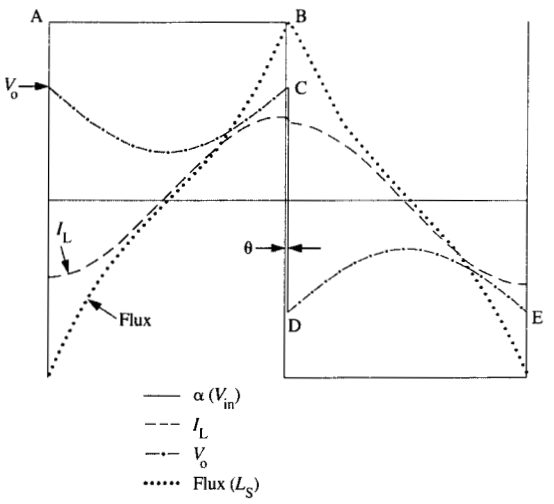

Figure 7

Time-domain plot of waveforms for conditions of high line voltage and minimum load; $\alpha = \alpha_{max}$; $Q = 0.05$; $\theta = 1.5°$; frequency = nominal.

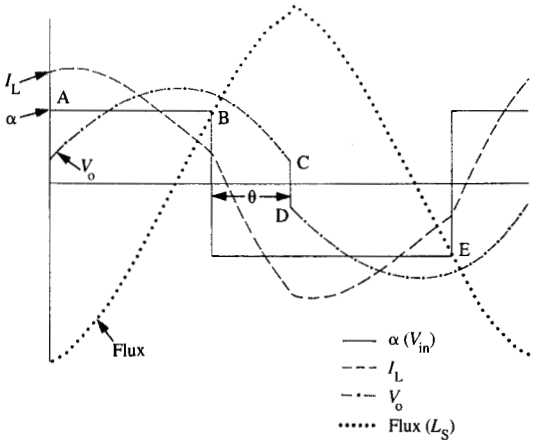

Figure 8

Time-domain plot of waveforms for conditions of low line voltage and maximum load; $\alpha = 0.4\,\alpha_{max}$; $Q = 0.5$; $\theta = 58°$; frequency = nominal.

• *Numerical methods*

The complexity of the transcendental exponential equations necessitates a numerical approach. A modified Newton-

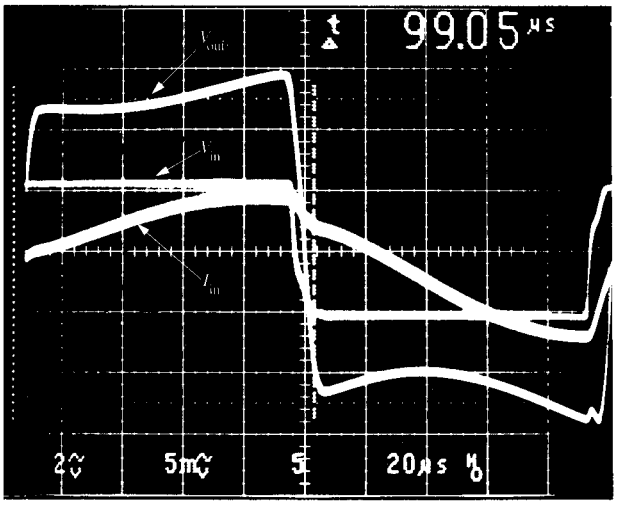

Figure 9

Experimental waveforms for conditions similar to those of Figure 6: $\alpha = 1.0$; $Q = 0.4$. The nominal input voltage was 5 V, or 158 "alpha units." Note that V_{in} is nearly in phase with I_{in}.

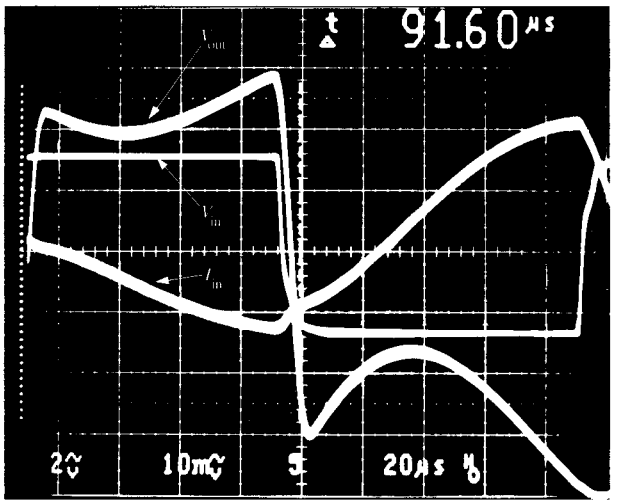

Figure 10

Experimental waveforms for conditions similar to those of Figure 7: $\alpha = 1.4$; $Q = 0.15$. The nominal input voltage was 5 V. Note the "corner peaks" in V_{out} and the polarity (phase) of the input current.

Raphson algorithm was selected and implemented with compiled BASIC on an IBM Personal Computer.* An arbitrary phase angle τ_θ was selected to minimize the difference $|f_1(\tau_\theta) - f_2(\tau_\theta)|$ over τ_θ, and substituted into the equations for the initial output voltage. The phase angle τ_θ was then incremented in the direction of convergence:

$$\tau_{\theta_2} = \tau_{\theta_1} - \Delta V/(\Delta V/\Delta\tau_\theta), \tag{27}$$

where ΔV is the difference in output equations for τ_{θ_1} and τ_{θ_2}, $\Delta\tau_\theta$ is the difference between τ_{θ_1} and τ_{θ_2}, and τ_{θ_1} and τ_{θ_2} are values of τ_θ initially chosen arbitrarily, then calculated.

This approach yields convergence of the two equations in typically four or fewer iterations. With the value of τ_θ determined, initial values of voltage and current can be determined, and complete time-domain plots can be obtained.

The program is written to prompt for normalized circuit constants such as input voltage, input frequency, and load (quality factor). The derivation of these quantities is shown in Appendix F for nominal conditions.

The program works well for a normal range of parameters, but convergence difficulties are encountered for extreme ranges. For example, a high line voltage with minimum load and a minimum line voltage with maximum load exhibit convergence difficulties. These results are closely corroborated by observed system behavior.

* Interview with Dr. Jorge Mescua, Department of Engineering Analysis and Design, University of North Carolina, Charlotte, NC.

Results

Plots of input and output waveforms can be obtained with variations in such parameters as input voltage and load. The results can be used to predict circuit performance as these parameters are varied. Figure 6 shows a condition of nominal line voltage, load, and frequency. (Magnitudes of the parameters are scaled for graphical reasons, since the magnitudes of the normalized parameters vary.) At nominal conditions, the input voltage and output voltage are rectangular. The phase angle is approximately 10° of the basic period. As expected, the flux is triangular. The shape of the output voltage gives a broad conduction angle for capacitive input filters. This can reduce the ripple current requirements for filters of this type. It is apparent from these waveforms that phasor techniques are not the appropriate tool for analysis.

Figure 7 is a plot of the same parameters for maximum line voltage and minimum load. The phase angle is reduced to approximately 1.5° and the output voltage has peaks. A capacitive input filter would tend to transfer these peaks to the output. The input current lags the input voltage and is larger in magnitude. This unusual effect is observed in physical systems.

Figure 8 shows the waveforms for minimum input voltage and maximum load. The phase angle is increased to 58° of the basic period, and the input current now leads the input voltage. The quasi-sinusoidal behavior of the waveforms indicates the approach of linear operation. If the input voltage is reduced or the load increased, we can force the

system to drop out of "resonance" and operate in a purely linear mode. (Authors such as Kakalec and Hart [6] use phasor analysis at the boundary between resonance and linear operation, noting that this is suggested by quasi-sinusoidal behavior near the transition.)

The plots of Figures 6–8 are in close agreement with experimental results (see **Figures 9–11**).

Under all conditions of line and load, the average output voltage is equal to 4.0 × Period (where Period is normalized to 1 for nominal conditions) for a given half-cycle. However, the distortion introduced indicates the need for an averaging filter for optimum results.

It is possible to derive a closed expression that closely approximates this relationship by assuming that both the input voltage and the output voltage are perfect square waves. The energy flow in the inductor may then be determined as a function of the phase angle between the two voltages and their amplitudes. From these results the following equation may be obtained:

$$\alpha_{\min} = \frac{64\pi Q_0}{\text{Period}}. \tag{28}$$

Figure 12 depicts a circuit for a higher-frequency ferroresonant supply. Q_1 and Q_2 provide a bipolar drive to transformer T_1. L_1 is a mutually coupled inductor that serves as the linear inductor. Due to impedance transformation, the equivalent capacitance C_1 is equal to $4C$ of our model.

Referring to Figures 6, 7, and 8 reveals some characteristics that enhance the use of this topology. For all conditions of line and load, input current lags input voltage at turn-off of the conducting device. If we observe the linear inductor dot convention, the current in the other device when it turns on is being supplied by the reactive bypass diode and is, in fact, negative with reference to the normal direction of current flow. This "dry" switching yields minimum switching losses. For FET-based designs, the parasitic diode which is inherent in these devices may be used for this purpose if speed and current ratings are adequate.

The turn-off condition as predicted by Figures 5 through 8 appears to be typical of inductive turn-off, which would lead to the coincidence of high power dissipation. In practice, however, this was not true; the devices Q_1 and Q_2 also turn off "dry," with their current falling to zero before the transistor voltage begins to rise. Subsequent evaluation has shown that this is due to the distributed shunt capacitance across the winding of the series inductor L_1. For example, as Q_1 begins to turn off, two new current paths are established (see **Figure 13**). The load current in the primary winding is shifted from the source to the resonant capacitor C_1, and the inductor current is shunted into the distributed capacitances C_{D1} and C_{D2}. Therefore, if the turn-off time of the devices Q_1 is less than the ring time of the inductor and its parasitic elements, the collector current will fall to zero before the collector voltage begins to rise. This performance characteristic can be controlled by fabricating the mutually coupled inductance for minimum distributed capacitance and adding a fixed capacitance in each inductor winding.

This low-dissipation switching is the most important aspect of the high-frequency ferroresonant concept, since

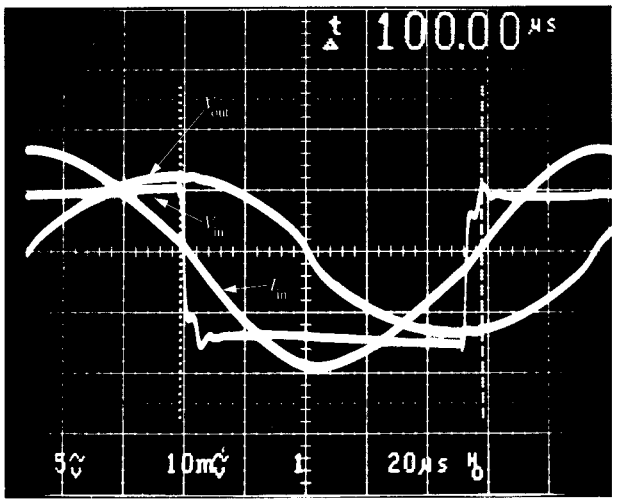

Figure 11

Experimental waveforms for conditions similar to those of Figure 8: $\alpha = 0.3$; $Q = 0.3$. The nominal input voltage was 2 V. Note the near-sinusoidal behavior of V_{out} and I_{in}, despite the "squareness" of V_{in}; note also that I_{in} is phase-inverted as compared with Figure 10.

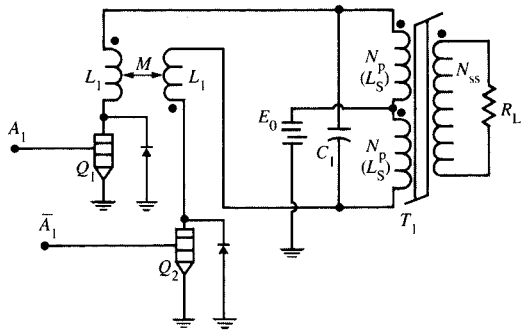

Figure 12

Possible implementation of a high-frequency ferroresonant regulator.

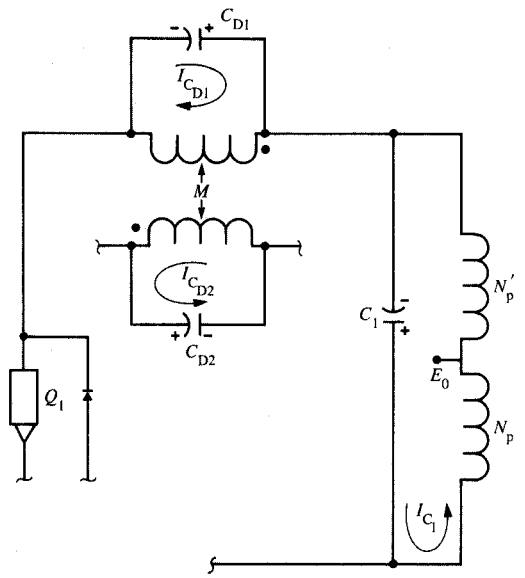

Figure 13

"Dry" switching of turn-off current.

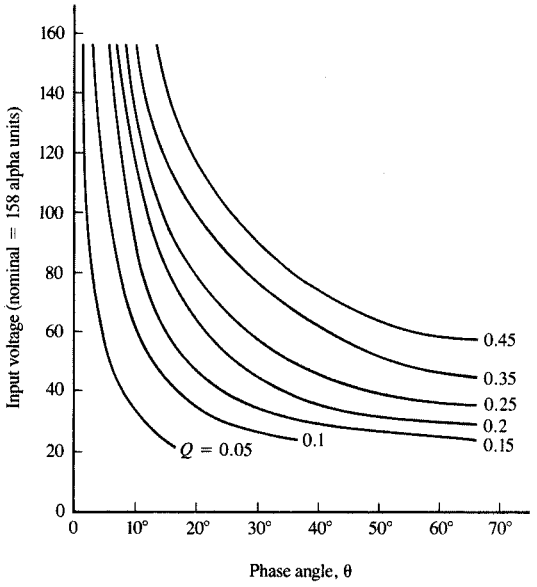

Figure 14

Input voltage versus phase angle with Q as a parameter.

switching-transistor device limitations have been a major cause of reliability concerns in off-line switching regulators.

The chief drawback to the use of higher-frequency ferroresonant supplies is the circulating currents that must be handled by the saturating core and capacitor. The peak current in the capacitor is inversely proportional to the characteristic impedance of the saturated inductor and capacitor. As the squareness ratio (the ratio of residual flux density to maximum flux density in the core) increases, the peak current also increases. For a given power level, the peak current will not be a function of frequency. Thus, a smaller capacitor will be required to handle the same RMS current as its 60-Hz cousin. The resulting core losses associated with the large currents must be addressed.

Parametric plots

Figure 14 shows a family of curves with Q as a parameter. The curves are hyperbolic and show increasing phase shift for decreasing line voltage or increased load. As θ approaches 90°, the circuit falls out of resonance.

Figure 15 shows a family of curves with input frequency as a parameter; this information might be used, e.g., to implement frequency modulation and thereby extend the useful operating range.

Since the results are normalized, they can be used both for a 60-Hz system and for higher-frequency designs. A higher operating frequency allows the use of smaller magnetic and capacitive devices.

Conclusions

This paper has reexamined the phenomenon of ferroresonance and derived a mathematical model that allows engineers to design and simulate ferroresonant circuits. The characterizing equations are general and may be used regardless of frequency, and the model is closely corroborated by experimental results. For a given power level and frequency, the relationships derived in this paper can be used to select values for all the elements in a ferroresonant power supply.

The ability of a ferroresonant unit to use a magnetic device as the regulating element is attractive from a reliability standpoint. The inherent regulation characteristics of the converter, along with its effective core utilization, make it a candidate for higher-frequency applications with the recent developments [13] in square-loop amorphous magnetics.

A high-frequency ferroresonant power supply and features unique to ferroresonance and the particular topology chosen have been discussed. These features allow "dry" switching of the transistors, yielding improved reliability.

To the authors' knowledge, a normalized design tool has not been available to accurately describe and simulate ferroresonant behavior under all circuit operating conditions. In addition, the mathematical approach used to solve this

system may be used for other mechanical or electrical systems which are nonlinear and can be described with a phase plane.

Appendix A: System equation solution

Given the expression

$$\alpha\tau + I_{Ln0} + \beta\chi_0 = \frac{d^2\chi}{d\tau^2} + 2Q_{n0}\frac{d\chi}{d\tau} + \beta\chi,$$

define

$$\chi = \underline{\chi} + \frac{I_{Ln0}}{\beta} + \chi_0$$

and then

$$\frac{d\chi}{dt} = \frac{d\underline{\chi}}{d\tau} \quad \text{and} \quad \frac{d^2\chi}{d\tau^2} = \frac{d^2\underline{\chi}}{d\tau^2},$$

so

$$\tau = \frac{d^2\underline{\chi}}{d\tau^2} + 2Q_{n0}\frac{d\underline{\chi}}{dt} + \beta\underline{\chi}.$$

To obtain a general solution, set

$$0 = \frac{d^2\underline{\chi}}{d\tau^2} + 2Q_{n0}\frac{d\underline{\chi}}{dt} + \beta\underline{\chi}.$$

This is a standard second-order equation, so the roots of the characteristic polynomial can be defined as

$$D = -Q_{n0} \pm j\sigma,$$

where

$$\sigma = \sqrt{\beta - Q_{n0}^2},$$

and the general solution for an underdamped homogeneous second-order linear differential equation can then be written as

$$\underline{\chi} = e^{-Q_{n0}\tau}(A\cos\sigma\tau + B\sin\sigma\tau).$$

Since the general differential equation has no power greater than τ, assume a particular solution in τ:

$$\underline{\chi}_p = K_0\tau + K_1;$$

then

$$\frac{d\underline{\chi}_p}{d\tau} = K_0 \quad \text{and} \quad \frac{d^2\underline{\chi}_p}{d\tau^2} = 0.$$

Substitution yields

$$\chi = e^{-Q_{n0}\tau}(A\cos\sigma\tau + B\sin\sigma\tau) + \frac{\alpha}{\beta}\tau - 2Q_{n0}\frac{\alpha}{\beta^2} + \frac{I_{Ln0}}{\beta} + \chi_0.$$

Using initial conditions $\tau = 0$, $\chi = \chi_0$, and $\dot{\chi} = V_{on0}$ to find A and B yields

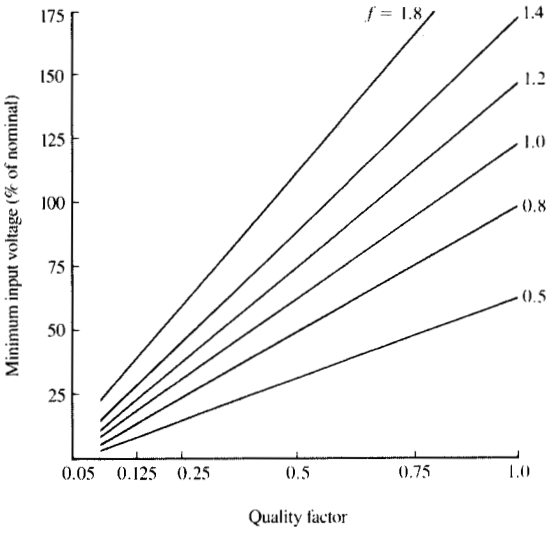

Figure 15

Minimum input voltage versus Q with frequency as a parameter.

$$\chi = e^{-Q_{n0}\tau}\left\{\left(\frac{2Q_{n0}\alpha}{\beta^2} - \frac{I_{Ln0}}{\beta}\right)\cos\sigma\tau + \frac{1}{\sigma}\left[V_{on0} - \frac{I_{Ln0}Q_{n0}}{\beta} + \frac{\alpha}{\beta}\left(\frac{2Q_{n0}^2}{\beta} - 1\right)\right]\sin\sigma\tau\right\} + \frac{\alpha}{\beta}\tau - \frac{2Q_{n0}\alpha}{\beta} + \frac{I_{Ln0}}{\beta} + \chi_0.$$

By using the product rule, the derivative is obtained:

$$\dot{\chi} = V_{on} = e^{-Q_n\tau}\left[\left(V_{on0} - \frac{\alpha}{\beta}\right)\cos\sigma\tau - \frac{1}{\sigma}\left(Q_{n0}V_{n0} + \frac{Q_{n0}\alpha}{\beta} - I_{Ln0}\right)\sin\sigma\tau\right] + \frac{\alpha}{\beta}.$$

Appendix B: Determining normalized inductor current

From the circuit schematic,

$$I_L = \frac{1}{L}\int [V_i(t) - V_o(t)]dt + I_{L0} = \frac{1}{L}\int V_i(t)dt - \frac{1}{L}\int V_o(t)dt + I_{L0}.$$

Since

$$\omega_0 t = 2\pi\tau$$

and

$$\int V_o(t)dt = N\psi_{max}(\chi - \chi_0),$$

we may substitute for t and $V_o(t)$

$$I_L = \frac{2\pi}{\omega_0 L}\int V_i(\tau)d\tau - (\chi - \chi_0)\frac{N\psi_{max}}{L} + I_{L0}.$$

Multiplying both sides by

$$\frac{4\pi^2 L}{N\psi_{max}} = \frac{4\pi^2}{N\psi_{max}\omega_0^2 C},$$

we have

$$\frac{I_L(4\pi^2)}{\omega_0^2 CN\psi_{max}} = \frac{8\pi^3 V_i(\tau)}{\omega_0 N\psi_{max}}\tau - 4\pi^2(\chi - \chi_0) + \frac{I_{L0}(4\pi^2)}{\omega_0^2 CN\psi_{max}}.$$

From earlier definitions of α and I_{Ln0},

$$I_{Ln} = \alpha\tau - 4\pi^2(\chi - \chi_0) + I_{Ln0}.$$

Appendix C: Phase-plane symmetry arguments

Refer to Figure 5. Several observations and assumptions can be made to simplify the analysis. If one assumes that this is a balanced magnetic system, the following statements hold true in steady state:

$$|I_{Ln0}| = |I_{Ln2}|;$$

$$|V_{on0}| = |V_{on2}|;$$

$$|I_{Lnx}| = |-I_{Lnx}|;$$

$$|V_{onx}| = |-V_{onx}|;$$

$$|I_{Ln1}| = |I_{Ln3}|;$$

$$|V_{on1}| = |V_{on3}|.$$

Next, if the saturated value of $L_S \ll L_L$, then the voltage reversal (points C − D) will occur in a time much less than the period of oscillation. Hence, the current in L_L cannot change much during this increment, so $I_{Ln1} = I_{Ln2}$ and $I_{Ln3} = I_{Ln0}$.

Furthermore, if one neglects winding and core losses during reversal, one can state that

$$|V_{on1}| = |V_{on2}|;$$

$$|V_{on3}| = |V_{on0}|.$$

Combining the above equations, we obtain

$$V_{on0} = V_{on1}$$

and

$$|I_{Ln0}| = |I_{Ln1}|.$$

The results imply that if we can describe the top segment of the phase trajectory, we have described the complete system. This allows the analysis of the top segment of the phase plane to completely describe the behavior of the system.

Appendix D: Derivation of the initial normalized linear inductor current

From Appendix B, recall that

$$I_{Ln} = \alpha\tau - 4\pi^2(\chi - \chi_0) + I_{Ln0}. \tag{D1}$$

Define τ_χ as the time required to move from point A to point B (see Figure 6). Then

$$I_{Ln\tau_\chi} = \alpha\tau_\chi - 4\pi^2[\chi_{\tau_\chi} - (-1)] + I_{Ln0}. \tag{D2}$$

Define τ_θ as the time required to move from point B to point C (see Figure 6). Then, by substitution in (D1),

$$-I_{Ln0} = -\alpha\tau_\theta - 4\pi^2(1 - \chi_{\tau_\chi}) + I_{Ln\tau_\chi}. \tag{D3}$$

Combining D1 and D2, we obtain

$$I_{Ln0} = 4\pi^2 - \frac{\alpha}{2}(\tau_\chi - \tau_\theta), \tag{D4}$$

but $\tau_\chi = [(\text{Period}/2) - \tau_\theta]$, where Period is the normalized period for one cycle (= 1 for nominal), so

$$I_{Ln0} = 4\pi^2 - \alpha\left(\frac{\text{Period}}{4} - \tau_\theta\right). \tag{D5}$$

Appendix E: Obtaining system solutions

From Appendix C, simplifying assumptions have been made that permit the treatment of the top segment of the phase plane to be sufficient to determine system behavior. Thus, the equations for flux, voltage, and current need to be applied only to this segment.

The trajectory in Figure 5 can be split into two linear segments: the segment between points A and B when the input and output voltage are in phase, and that between points B and C when the input switches and is out of phase.

The flux and voltage equations (22) and (23) can be combined with the inductor current equations to generate equations for the initial output voltage V_{on0} that are functions of known coefficients and time.

This is accomplished by rewriting the flux and voltage equations in the form

$$\left.\begin{aligned} &\chi = K_1 V_{on0} + K_2 I_{Ln0} + K_3, \\ &V_{onx} = K_4 V_{on0} + K_5 I_{Ln0} + K_6, \\ &\text{and} \\ &\tau_{final} = \frac{T}{2} - \tau_\theta. \end{aligned}\right\} \text{segment A} - \text{B}.$$

Similarly, the second segment may be written as

$$\left.\begin{aligned} V_{on1} &= V_{on0} \text{ (Appendix C)} \\ &= K_7 V_{onx} + K_8 I_{Lnx} + K_9, \\ 1 &= K_{10} V_{onx} + K_{11} I_{Lnx} + K_{12}, \\ &\text{and} \\ \tau_{Final} &= \tau_\theta. \end{aligned}\right\} \text{segment B} - \text{C}.$$

These equations, coupled with the inductor current equations (D1), (D3), and (D4), are solved by substitution to yield two expressions for V_{on0} that are functions of $\pm\ \alpha$, β, Q_{n0}, Period, and τ_θ. Since α, β, Q_{n0}, and Period are design parameters and hence known, we can write the two equations and solve for τ_θ.

Substitution yields the following equations:

$$V_{on0} = \frac{(K_7K_5 - 4\pi^2K_8K_2)\left[4\pi^2 - \alpha\left(\frac{\text{Period}}{4} - \tau_\theta\right)\right]}{1 - K_7K_4 + 4\pi^2K_8K_1} + \frac{K_7K_6 + K_8\alpha\left(\frac{\text{Period}}{4}\right) + K_{13}}{1 - K_7K_4 + 4\pi^2K_8K_1},$$

where $K_{13} = -4\pi^2K_8K_3 + K_9$; and

$$V_{on0} = \frac{1 + K_3(4\pi^2K_{11} - 1) - K_{10}K_6 - \alpha K_{11}\left(\frac{\text{Period}}{4}\right) - K_{12}}{K_1(1 - 4\pi^2K_{11}) + K_{10}K_4} + \frac{[K_2(4\pi^2K_{11} - 1) - K_{10}K_5]K_{14}}{K_1(1 - 4\pi^2K_{11}) + K_{10}K_4},$$

where $K_{14} = 4\pi^2 - \alpha[(\text{Period}/4) - \tau_\theta]$.

The equations above are solved by varying τ_θ until both equations converge to the same value.

With τ_θ determined, I_{Ln0} can be calculated. With these two parameters known, along with the initial normalized flux (-1), the flux, voltage, and current equations can be plotted for an entire cycle.

Appendix F: Derivation of nominal normalized circuit coefficients

Derivation of α, β, and Q:

1. α is defined as

   $$\frac{8\pi^3V_i}{N\omega_0\psi_{max}}.$$

   Since V_i must supply volt-seconds to saturate the core (+ to − saturation in a half-cycle),

   $$\frac{V_i}{\omega_0} = 2N\psi_{max},$$

   and let

   $$\frac{V_i}{\omega_0} = 2\pi\left(\frac{\tau}{2}\right)V_i,$$

   or

   $$\left(\frac{2\pi\tau}{2}\right)V_i = 2N\psi_{max};$$

   $$\frac{V_i\tau}{N\psi_{max}} = \frac{2}{\pi}.$$

   Substituting,

   $$\alpha = 8\pi^3 \times \frac{2}{\pi} = 158 \text{ (nominal value of } \alpha).$$

2. β is defined as

   $$\frac{4\pi^2(\omega_0^2 + W_S^2)}{\omega_0^2}.$$

   For the segment of interest,

   $$W_S^2 = \frac{1}{L_SC} \ll \omega_0^2 = \frac{1}{L_LC},$$

   so

   $$\beta = 4\pi^2 \text{ (nominal value of } \beta).$$

3. Period and frequency were normalized to 1 by definition in the section on circuit normalization.
4. Q was found to be optimum at 0.2 from experimental data (see Figure 15).

References and note

1. L. Teschler, "Power Supplies Gain Improvement from IC Technology," *Machine Design* **57,** No 11, 119–123 (May 23, 1985).
2. "High-Frequency Converters," *Proceedings of the IEEE Applied Power Electronics Conference*, Session III, pp. 105–165 (1987).
3. *Unitrode Power Supply Design Seminar*, Unitrode Corporation, Lexington, MA, 1984.
4. R. N. Basu, "A New Approach in the Analysis and Design of the Ferroresonant Transformer," *IEEE Trans. Magnetics* **MAG-3,** 43–49 (1967).
5. I. B. Friedman, "The Analysis and Design of Ferromagnetic Circuits," *IRE Trans. Component Parts* **CP-3,** 11–14 (1956).
6. R. J. Kakalec and H. P. Hart, "The Derivation and Application of Design Equations for Ferroresonant Voltage Regulators and Rectifiers," *IEEE Trans. Magnetics* **MAG-7,** 205–211 (1971).
7. J. T. Keefe, "Static Magnetic Regulator Solves Transient Voltage Problem," *Canadian Electronics Engineering* **4,** 28–31 (1960).
8. B. C. Biega, "Practical Equivalent Circuits for Electromagnetic Devices," *The Electronic Engineer* **26,** 52–56 (1967).
9. *SPICE Version 2.G User's Guide* (August 10, 1981), Department of Engineering and Computer Science, University of California at Berkeley, Berkeley, CA 94720.
10. *ASTAP Reference Guide*, SH20-1118-00, IBM Corporation; available through IBM branch offices.
11. M. Tabrizi, "The Nonlinear Magnetic Core Model Used in SPICE PLUS," *Proc. IEEE Applied Power Electronics Conference*, pp. 32–36 (1987).
12. *Solid State Magnetic and Dielectric Devices*, H. W. Katz, Ed., John Wiley & Sons, Inc., New York, 1959.
13. One recently developed amorphous square-loop material is Metglass® Alloy 2714A, a product of Allied Chemical Corp., Morristown, NJ. Data on this product can be found in *Allied Metglass Products Catalog*, 1986, Allied Metglass Products, Parsippany, NJ 07054, telephone (201) 455-7691.

Received March 4, 1987; accepted for publication November 1, 1987

Donald M. Scoggin *IBM Corporation, P.O. Box 12195, Research Triangle Park, North Carolina 27709.* Mr. Scoggin is a staff engineer in electrical component engineering. He received a B.S.E.E. in 1977 from North Carolina State University, Raleigh, and an M.S.E. in 1986 from the University of North Carolina at Charlotte. Since joining IBM in 1978, Mr. Scoggin has worked in the design, qualification, and testing of power supplies. He is a member of the IEEE.

James E. Hall, Jr. *IBM Corporation, P.O. Box 12195, Research Triangle Park, North Carolina 27709.* Mr. Hall is a staff engineer in power systems. He received a B.S.E.E. in 1961 and an M.S.E.E. in 1967 from Duke University, Durham, North Carolina. Prior to joining IBM, Mr. Hall was involved in the design of switching regulator power supplies for NASA. Since joining IBM in 1967, he has worked in the areas of power and circuit technology. His recent activity has been the design of power supplies for telecommunication products.